

Optically-controlled logic gates for two spin qubits in vertically-coupled quantum dots

C. Emary* and L. J. Sham

Department of Physics, University of California San Diego, La Jolla, CA 92093, U.S.A.

(Dated: July 29, 2021)

We describe an interaction mechanism between electron spins in a vertically-stacked double quantum dot that can be used for controlled two-qubit operations. This interaction is mediated by excitons confined within, and delocalized over, the double dot. We show that gates equivalent to the $\sqrt{\text{SWAP}}$ gate can be obtained in times much less than the exciton relaxation time and that the negative effects of hole-mixing and spontaneous emission do not seriously affect these results.

PACS numbers: 78.67.Hc, 03.67.Lx

The spin of an electron confined in a quantum dot (QD) is one of the leading candidates for the realization of a practical qubit. Since the work of Loss and DiVincenzo [1], there have been a number of proposals on how best to achieve the precise manipulations of such spins required for the operation of quantum logic. See, for example, [2, 3, 4, 5].

Whilst interest in electrostatic gating remains strong, the use of lasers has several advantages in this role, most notably speed and control. Despite significant theoretical advances in this direction, there has, as yet, been no experimental demonstration of optically-controlled gating between electron spins in QDs.

In this paper, we describe an interaction mechanism to achieve just this. This qubit-qubit interaction is mediated by interdot tunnelling of photo-excited carriers — an area which has been the subject of significant recent experimental advances [6, 7]. Our results are of explicit relevance to the current generation of vertically-stacked self-assembled InAs QDs, but are also easily adaptable to the other dots, including horizontally-coupled ones.

The interaction we describe has its origin in the so-called optical-RKKY effect, in which two electron spins are coupled via their exchange interactions with optically-generated excitons in the semiconductor bulk [8]. The coupling effect of these bulk excitons between two electron spins in a double QD was examined in Ref. [9]. Here we consider an interaction mediated, not by bulk excitons, but by a single exciton confined in the same double QD structure. We describe a situation in which the excitonic electron is able to tunnel between the dots and form delocalized ‘molecular’ states. It is the exchange interaction between this electron and the resident qubit electrons that leads to an optically controlled gating. This gate, although not one of the standard quantum computation (QC) gates, can be used to form a controlled- Z operation when used twice in conjunction with single qubit rotations, and is, in this way, similar to the $\sqrt{\text{SWAP}}$ gate.

The main factor limiting the speed with which oper-

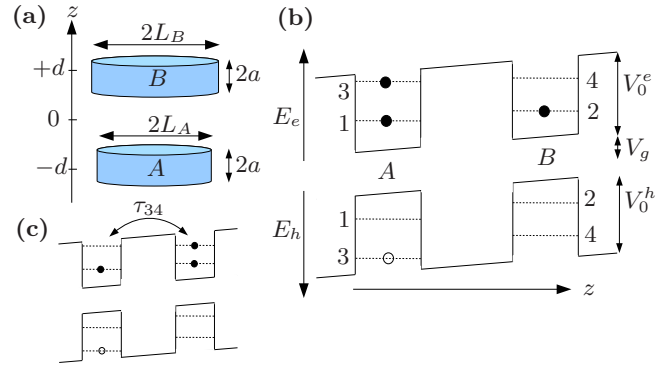


FIG. 1: (colour online) (a) Sketch of the two vertically-stacked quantum dots. Growth direction is the z direction and the two dots are positioned symmetrically at $z = \pm d$. The dots have heights $2a$ and the width of the barrier between them is $b \equiv 2(d - a)$. The lower (A) and upper (B) dots have Darwin radii of L_A and L_B respectively. (b) Two electronic and two hole levels in each dot take part in gate operation. The lowest electron levels in each dot (labeled 1 and 2) are the two qubit levels and an electron permanently resides in each of them. Laser illumination is tuned such that it creates an exciton in the excited levels of dot A only (levels 3). (c) Due to a tunnel coupling τ_{34} between the dots and a resonance condition met through the tuning of the gate voltage V_g , the excitonic electron can tunnel back-and-forth. The exchange interaction between this electron and the qubits gives rise to the optically-induced interaction between the qubits that can be used to perform a quantum gate.

ations can be performed in this set-up comes from the ‘kinetic exchange’ between qubit spins which arises from the virtual tunneling of the qubit electrons between dots. This is an important consideration in vertically-stacked dots, and we show here that by choosing appropriate dot parameters, we can make this effect small and still obtain fast two-qubit operations.

Our proposal therefore offers an accessible path to the demonstration of quantum logic in the solid state. Furthermore, it offers insight into the dynamics of interacting few-body systems in confined nanostructures — a topic of increasing experimental relevance.

Figure 1 illustrates the basic principle at work here.

*Present address: Institut für Theoretische Physik, TU Berlin, Hardenbergstr. 36, D-10623 BERLIN.

The two qubit electrons reside, one a piece, in the ground-state levels of a vertical double-dot structure. The dots have slightly different diameters and a static gate voltage V_g is applied in the growth direction. The distance between the dots is small enough that tunneling can occur between the dots, but large enough to suppress the direct exchange interaction between the two qubit electrons. The tunneling of the qubit electrons into each others dot is strongly suppressed by the energy required to doubly charge one of the dots.

A circularly-polarized laser pulse is used to generate an exciton into the lowest excited orbitals of dot A as shown in Fig. 1b. The gate voltage is tuned such that the energy of this three-electron-and-one-hole configuration is resonant with that shown in Fig. 1c, where the excited electron is in dot B.

The resonant tunneling of the electron between these configurations creates a set of hybridised states in which the excitonic electron is delocalized over both dots. The qubit electrons experience a strong intradot exchange interaction with this delocalized electron and this mediates an effective interaction between the two qubits. By controlling the laser parameters, this interaction can be harnessed to perform quantum logic operations.

We begin our detailed treatment by describing the single-particle states of the double dot. This includes a calculation of the size of the interdot tunneling elements. For reasonable dot separations we describe a situation where the qubits in the ground states are effectively isolated from one another, but where the exciton electron is free to tunnel. We then detail the spectrum of the four-body system resulting from the interplay of confinement, tunneling and the Coulomb interaction. From this follows the quantum logic properties of the system. Analytically, we derive an effective gate operator for the system under adiabatic conditions. We also use numerics to explore the non-adiabatic capabilities. We show that gates equivalent to the $\sqrt{\text{SWAP}}$ gate can be obtained in times much less than the exciton relaxation time and that the negative effects of hole-mixing and spontaneous emission do not seriously affect these results.

I. SINGLE-PARTICLE STATES

The potential experienced by a conduction band (CB) electron in the double-dot structure may be approximated as follows. In the growth direction z we have a double square-well potential with wells of width $2a$ and depth V_0 centred at $\pm d$:

$$V_z(z) = \begin{cases} 0 & |z \pm d| \leq a, \\ V_0 & \text{otherwise.} \end{cases} \quad (1)$$

The width of the barrier between the dots (the parameter often quoted in experiments) is given by $b \equiv 2(d - a)$. Confinement in the x - y plane is assumed harmonic with different confinement energies above and below the $z = 0$

plane corresponding to dots A and B :

$$V_\rho(\mathbf{r}) = \begin{cases} 1/2 m_e \omega_A^2 \rho^2 & z < 0, \\ 1/2 m_e \omega_B^2 \rho^2 & z \geq 0. \end{cases} \quad (2)$$

Here, $\rho = \sqrt{x^2 + y^2}$ is the radial coordinate, m_e is effective mass of the CB electron, and $\hbar\omega_X = \hbar^2/(m_e L_X^2)$ is the confinement energy of dot $X = A, B$. The Hamiltonian of the electron is then

$$H_{\text{CB}} = \frac{1}{2m_e} \mathbf{p}^2 + V_z(z) + V_\rho(\mathbf{r}) + E_g. \quad (3)$$

where E_g is the band-gap.

We will consider the two dots to be separated such that a variational treatment in terms of wave functions localized in each of the individual dots is appropriate. Let us label with 1 and 3 the lowest two levels in dot A , and with 2 and 4 those in dot B . Our starting point, then, is the set of four single-particle wave functions

$$\begin{aligned} \phi_1(\mathbf{r}) &= \chi(z+d)\eta_s(\omega_A; \rho, \theta), \\ \phi_2(\mathbf{r}) &= \chi(z-d)\eta_s(\omega_B; \rho, \theta), \\ \phi_3(\mathbf{r}) &= \chi(z+d)\eta_p(\omega_A; \rho, \theta), \\ \phi_4(\mathbf{r}) &= \chi(z-d)\eta_p(\omega_B; \rho, \theta). \end{aligned} \quad (4)$$

In the growth direction, $\chi(z \mp d)$ are square-well eigenfunctions centred at $z = \pm d$. In the xy plane, the functions $\eta_s(\omega_X; \rho, \theta)$ and $\eta_p(\omega_X; \rho, \theta)$ describe the ground and first-excited Fock-Darwin wave functions for confinement energy ω_X . These wave functions are given explicitly in Appendix A. This set of wave functions is not orthogonal since, although the overlaps $S_{12} = \langle \phi_1 | \phi_2 \rangle$ and $S_{34} = \langle \phi_3 | \phi_4 \rangle$ are small, they are finite. We thus use their orthogonalized counterparts $\psi_i(\mathbf{r})$ as outlined in the Appendix.

The evaluation of the Hamiltonian of Eq. (3) in this orthogonal basis gives us our approximate single CB-electron Hamiltonian. Correct to first order in the overlaps $S_{12} \approx S_{34}$, we have

$$H_{\text{CB}} = \begin{pmatrix} E_1 & -\tau_{12} & 0 & 0 \\ -\tau_{12} & E_2 + V_g & 0 & 0 \\ 0 & 0 & E_3 & -\tau_{34} \\ 0 & 0 & -\tau_{34} & E_4 + V_g \end{pmatrix}. \quad (5)$$

The diagonal energies are given by

$$\begin{aligned} E_1 &= E_z + E_g + \hbar\omega_A; & E_2 &= E_z + E_g + \hbar\omega_B; \\ E_3 &= E_z + E_g + 2\hbar\omega_A; & E_4 &= E_z + E_g + 2\hbar\omega_B, \end{aligned} \quad (6)$$

where E_z is the energy resulting from the z confinement and is the same for both dots.

The quantities τ_{12} and τ_{34} are ground- and excited-state tunneling amplitudes. They may be approximated as

$$\tau_{12} \approx \tau_{34} \approx 4aV_0BC \frac{L_A L_B}{L_A^2 + L_B^2} e^{-2\beta d}, \quad (7)$$

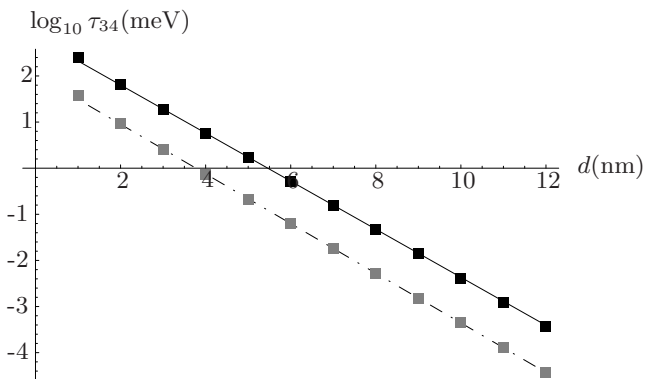


FIG. 2: Logarithm of τ_{34} , the tunneling amplitude between excited states in different dots as a function of the interdot distance d . The solid black line shows the approximate result of Eq. (7) and the black points show a numerical evaluations of full single-particle matrix element. The dashed line and grey boxes show the analogous quantities for heavy-hole tunneling. The dot height is $2a = 2$ nm and the radial confinement energies were $\hbar\omega_A^e = 35$ meV and $\hbar\omega_B^e = 30$ meV for all carriers. The vertical confinement depth was $V_0^e = 680$ meV for electrons and $V_0^h = 100$ meV for holes. We took the electron mass to be $0.04m_0$ in InAs and $0.067m_0$ in the surrounding GaAs matrix. Heavy holes were masses $m_{hz} = 0.34m_0$ and $m_{h\perp} = 0.04m_0$ for both InAs and GaAs.

where β , B , and C are functions of V_0 determined by the continuity of the z -direction wave function (see appendix). The dependence of τ_{34} on the interdot distance is illustrated in Fig. 2 for typical parameters. Current experiments have largely operated at small interdot spacings where the tunneling is large. For example, Ortner and coworkers [6] measured a value of $\tau_{12} \approx 13$ meV for $d \approx 3.5$ nm, which is in good agreement with the results plotted in Fig. 2. For our purposes, we require a much smaller tunneling such that localized states are still well defined. We will consider separations in the range of $d \approx 8$ nm ($b \approx 14$ nm), where the tunneling amplitude lies in the range 10-100 μ eV.

In Eq. (5) we have also taken into account the effects of the gate voltage applied in the z direction by incorporating a first-order shift in the energy levels of dot B by an amount V_g [7].

In InAs dots, the valence-band states have a predominantly heavy-hole (HH) character. The single-particle Hamiltonian for such holes follows in exactly the same way as above except that the parameters differ. In particular, the HH mass in the growth direction, m_{hz} , is different to that in the xy plane $m_{h\perp}$. The heavier mass of the HH in the z direction, as compared with the electron, means that the HHs are more localized than the electrons. This in turn means that the HH tunneling amplitudes between the dots are approximately one order of magnitude smaller than those for the electrons, as illustrated in Fig. 2.

II. LIGHT-MATTER INTERACTION

The multi-particle basis states for our problem are chosen by filling the appropriate single-particle levels. Prior to the application of the laser, there are two electrons in the system and these reside in the ground-state levels of the dots. Interaction with the laser generates an additional electron-hole pair in the excited-levels of the double-dot system.

We consider here illumination with a σ_+ circularly polarized laser propagating in the growth direction. Conservation of angular momentum means that this excites an exciton consisting of a spin-down electron and a spin-up heavy hole. Here, we have neglected hole-mixing and assumed that the in-plane magnetic field is zero — points which we return to later. The laser is tuned such that it creates the exciton in the excited levels of the dots and not in the ground-state levels where the qubit electrons reside. In principle, illumination can create an exciton with a hole in either dot

The block structure of the Hamiltonian for the interacting system reads

$$H_{\text{total}} = \left(\begin{array}{ccc|cc} X^{(D)} & T_{X4}^e & T_{X3}^e & 0 & \Omega^{(D)} \\ T_{X4}^{e\dagger} & X^{(4)} & T^h & \Omega^{(4)} & 0 \\ T_{X3}^{e\dagger} & T^{h\dagger} & X^{(3)} & \Omega^{(3)} & 0 \\ \hline 0 & \Omega^{(4)\dagger} & \Omega^{(3)\dagger} & G & T_G^e \\ \Omega^{(D)\dagger} & 0 & 0 & T_G^{e\dagger} & D \end{array} \right). \quad (8)$$

The two blocks in the bottom righthand corner, G and D , describe states consisting of the two resident electrons only — in G the electrons are separated one in each dot; in D , one of the dots is doubly occupied. These two blocks are coupled via the electron-tunneling terms of block T_G^e . The blocks $X^{(3)}$ and $X^{(4)}$ describe states with two resident electrons plus the exciton, with the superscript referring to the dot-level in which the hole is located. These two blocks are coupled by the hole-tunneling terms of block T^h . Block $X^{(D)}$ describes states where an exciton is present and one of the ground-state levels is doubly occupied. This block is coupled to the other exciton-containing states through the electron tunneling blocks $T_{X3,4}^e$. Finally, the blocks $\Omega^{(i)}$; $i = 3, 4, D$ contain the light-matter interaction terms, and provide the connexion between the ground and excited sectors. It should be noted that the effects of Coulomb interaction are incorporated into the diagonal blocks of H_{total} , and that the exciton blocks, $X^{(i)}$ also contain single-electron tunneling terms.

We can make several approximation that reduce the complexity of H_{total} significantly. Firstly we assume that, whereas in principle the laser can excite an electron hole-pair in either of the dots, we assume that the two dots are sufficiently distinct in size that, in fact they are only generated in dot A . We will later chose the difference in confinement energies of the two dots to be ≈ 5 meV, so this is certainly valid. We can also neglect the generation of the indirect excitons such as $e_{3\downarrow}^\dagger h_{4\uparrow}^\dagger$, as these have very

small transition matrix elements. This means that the light-matter interaction is well approximated as

$$H_{\text{int}} = \Omega(t)e^{-i\omega t}e_{3\downarrow}^\dagger h_{3\uparrow}^\dagger + \text{H.c.}, \quad (9)$$

where $\Omega(t)$ is the time-dependent Rabi frequency of the exciton transition. The block $\Omega^{(4)}$, corresponding to the generation of excitons in dot B , is therefore zero. Furthermore, hole-tunneling is very effectively suppressed in this system — not only are the hole-tunnelling matrix elements much smaller than their electronic counterparts (see previous section), but under the operating conditions of our device, to be described below, these transitions are far off-resonant. We therefore treat the block $X^{(4)}$, with a hole in dot B , as being effectively decoupled from the dynamics that we are interested in.

Finally, transitions to states in which the dot levels are doubly occupied are suppressed by the enhanced Coulomb interaction of such states. That this is still the case even with different dot sizes and in the presence of applied field is justified in the next section. This means that the blocks D and X^D are decoupled from the rest of the system over the relevant timescales. Taken together, these approximations mean that the system can be described with just the portion of the Hamiltonian H_{total} consisting of the blocks G , $X^{(3)}$ and $\Omega^{(3)}$. Since these blocks have significant internal structure themselves, the solution of this problem is still by no means trivial.

III. GROUND-STATE SECTOR: ISOLATED QUBITS

We continue our treatment by temporarily reinstating block D and consider all states in which there are only two electrons in the system. This is the “ground-state sector”, and is described by blocks G , D and T_G^e above. It is clear that only states with one electron in each dot represent good two-qubit states and that double-occupancy

of either dot, as in block D , is a source of error. It is therefore the purpose of this section to describe this sector and to show the extent to which block D can be neglected and the qubits thought of as isolated.

We can decompose the proper qubit sector as $G = \text{Diag}\{G_{-1}, G_0, G_{+1}\}$, where the subblocks are labelled by the z -projection of the total electron spin. Block G_{-1} corresponds to the energy of the two-qubit state $e_{1\downarrow}^\dagger e_{2\downarrow}^\dagger|0\rangle$, G_{+1} corresponds to $e_{1\uparrow}^\dagger e_{2\uparrow}^\dagger|0\rangle$, and G_0 consists of the two qubit states with the electrons having opposite spins: $e_{1\downarrow}^\dagger e_{2\uparrow}^\dagger|0\rangle$ and $e_{1\uparrow}^\dagger e_{2\downarrow}^\dagger|0\rangle$.

The exclusion principle determines that there are only two states in block D , namely $e_{1\downarrow}^\dagger e_{1\uparrow}^\dagger|0\rangle$ and $e_{2\downarrow}^\dagger e_{2\uparrow}^\dagger|0\rangle$. Conservation of electron spin angular momentum means that only block G_0 couples to the block D . We can therefore consider the effects of double occupancy by concentrating on the following Hamiltonian

$$H_{GD} = \begin{pmatrix} G_0 & T_G^e \\ T_G^e & D \end{pmatrix}, \quad (10)$$

each block of which is a two-by-two-matrix.

To assess the effects of double occupancy it is necessary to consider the Coulomb interaction between the confined carriers, in this case electrons. The electron-electron matrix elements between single-particle orbitals are given by

$$V_{ijkl}^{eeee} = E_C \int d^3\mathbf{r}_1 d^3\mathbf{r}_2 \frac{\psi_i^e(\mathbf{r}_1)\psi_j^e(\mathbf{r}_2)\psi_k^e(\mathbf{r}_2)\psi_l^e(\mathbf{r}_1)}{|\mathbf{r}_1 - \mathbf{r}_2|}, \quad (11)$$

with $E_C = e^2/(4\pi\epsilon_0\epsilon_R)$. We define similar quantities V_{ijkl}^{ehhe} for electron-hole interactions and will only consider electron-hole direct interaction as e - h exchange effects are negligible.

Including both Coulomb interactions and single-particle terms, the Hamiltonian of the ground-state sector in question is

$$H_{GD} = \begin{pmatrix} E^G + V_g & J_{12} & & -\tau_{12}^e & & & & -\tau_{12}^e \\ J_{12} & E^G + V_g & & \tau_{12}^e & & & & \tau_{12}^e \\ -\tau_{12}^e & \tau_{12}^e & E^G - V_{1221}^{eeee} + V_{1111}^{eeee} - \Delta E & & & & & 0 \\ -\tau_{12}^e & \tau_{12}^e & & 0 & & & & E^G - V_{1221}^{eeee} + V_{2222}^{eeee} + \Delta E + 2V_g \end{pmatrix}, \quad (12)$$

where we have defined $E^G = E_1^e + E_2^e + V_{1221}^{eeee}$, $\Delta E = E_2^e - E_1^e$, and $J_{12} = V_{1212}^{eeee}$ is the magnitude of ground-state exchange interaction. This exchange term can be approximated as

$$J_{12} \approx \frac{8E_C\sqrt{\pi}C^4}{L_A^2 L_B^2 (L_A^{-2} + L_B^{-2})^{3/2}} (d-a)^2 e^{-4\beta d}. \quad (13)$$

For the dot separations in which we are interested here ($d \approx 8$ nm), this exchange energy is of the order 10^{-5} meV and can thus be neglected.

The tunneling amplitude τ_{12} means that double-occupancy of the qubit levels can, in principle, occur, and this would clearly be deleterious. However, if the doubly occupied states are much higher in energy than the singly-occupied ones, double occupancy will be sup-

pressed. This requires that the energy differences satisfy

$$\begin{aligned} Q_1 &\equiv V_{1111}^{eeee} - V_{1221}^{eeee} - \Delta E - V_g \gg \tau_{12}^e, \\ Q_2 &\equiv V_{2222}^{eeee} - V_{1221}^{eeee} + \Delta E + V_g \gg \tau_{12}^e. \end{aligned} \quad (14)$$

With these inequalities satisfied, the effect of double occupancy is reduced to imparting a small residual ‘kinetic exchange’ interaction on the fixed qubits. To second order in τ_{12} this kinetic exchange energy may be approximated as τ_{12}^2/Q , with $Q^{-1} = Q_1^{-1} + Q_2^{-1}$. The important time-scale,

$$T_Q = \hbar Q / \tau_{12}^2, \quad (15)$$

follows accordingly such that, for times $t \ll T_Q$, the qubits are effectively isolated from one another.

We will see later that device operation requires that the offset V_g should be set as

$$\begin{aligned} V_g &= E_3^e - E_4^e + V_{1331}^{eeee} - V_{2442}^{eeee} + V_{2332}^{eeee} - V_{1441}^{eeee} \\ &\quad + V_{4334}^{ehhe} - V_{3333}^{ehhe} + J_{24} - J_{13}. \end{aligned} \quad (16)$$

As the Coulomb elements are approximately symmetric between the dots, we can approximate Q_i as

$$\begin{aligned} Q_1 &\approx V_{1111}^{eeee} - V_{1221}^{eeee} + V_{3333}^{ehhe} - V_{4334}^{ehhe} + \Delta E, \\ Q_2 &\approx V_{2222}^{eeee} - V_{1221}^{eeee} - V_{3333}^{ehhe} + V_{4334}^{ehhe} - \Delta E. \end{aligned} \quad (17)$$

In order to obtain as long a time T_Q as possible, we need to maximize Q , and this is achieved when $Q_1 = Q_2$. This in turn means that the optimal difference between the confinement energies of the two dots should

be $\Delta E \approx -V_{3333}^{ehhe} + V_{4334}^{ehhe}$, in which case $Q = Q_1/2 \approx 1/2(V_{1111}^{eeee} - V_{1221}^{eeee})$. Typical parameters give $\Delta E \approx Q \approx 5$ meV and thus $T_Q = 1.3$ ns for a tunneling amplitude of $\tau_{12} = 0.05$ meV, and $T_Q = 82$ ps for $\tau_{12} = 0.2$ meV. Providing then that the operation of our gate is much faster than T_Q , we can neglect the effects of double occupancy in the ground-state sector. A similar analysis shows that tunneling of ground-state electrons is suppressed to a similar degree also in the presence of the exciton. This means that, with the above proviso, we are justified in neglecting blocks D and X^D from H_{total} .

The other important time-scale for this system is the relaxation rate of the exciton. Experiments have shown that this quantity is of the order of $T_{\text{rel}} \approx 1$ ns or greater [10, 11]. This, therefore, is of the same order of magnitude as T_Q for $\tau_{12} = 0.05$ meV.

IV. EXCITON STATES

We now consider states with the exciton, and since the hole is always localized in state 3, we consider only block $X^{(3)}$. We can decompose this block into subsectors based on the z -projection of the total electron spin: $X^{(3)} = \text{Diag} \{ X_{3/2}^{(3)}, X_{1/2}^{(3)}, X_{-1/2}^{(3)}, X_{-3/2}^{(3)} \}$. Since there are no spin-flip processes effective over the time scale of a typical gate operation, these sectors are independent and each excitonic sector couples exclusively to one of sub-blocks of G . This means that the total Hamiltonian for the system can be written

$$H_{\text{total}} = \begin{pmatrix} X_{-3/2}^{(3)} & \Omega_{-3/2}^{(3)} & 0 & 0 & 0 & 0 & 0 \\ \Omega_{-3/2}^{(3)\dagger} & G_{-1} & 0 & 0 & 0 & 0 & 0 \\ \hline 0 & 0 & X_{-1/2}^{(3)} & \Omega_{-1/2}^{(3)} & 0 & 0 & 0 \\ 0 & 0 & \Omega_{-1/2}^{(3)\dagger} & G_0 & 0 & 0 & 0 \\ \hline 0 & 0 & 0 & 0 & X_{1/2}^{(3)} & \Omega_{1/2}^{(3)} & 0 \\ 0 & 0 & 0 & 0 & \Omega_{1/2}^{(3)\dagger} & G_{+1} & 0 \\ \hline 0 & 0 & 0 & 0 & 0 & 0 & X_{+3/2}^{(3)} \end{pmatrix} \quad (18)$$

Let us label each of these interacting sub-blocks with the electron-spin projection of the exciton state. We therefore have $H_{\text{total}} = \text{Diag} \{ H^{(-3/2)}, H^{(-1/2)}, H^{(1/2)}, H^{(3/2)} \}$. Block $H^{(3/2)}$ is clearly decoupled from the dynamics of the system and can be ignored.

Let us consider the sector described by $H^{(-3/2)}$, in which both qubits are spin-down and thus parallel to the electronic spin of the exciton. Only three states

then make up this sector: the photo-excited state $|\text{I}\rangle = e_{1\downarrow}^\dagger e_{2\downarrow}^\dagger e_{3\downarrow}^\dagger h_{3\uparrow}^\dagger |0\rangle$, the same configuration but with the electron tunnelled $|\text{II}\rangle = e_{1\downarrow}^\dagger e_{2\downarrow}^\dagger e_{4\downarrow}^\dagger h_{3\uparrow}^\dagger |0\rangle$, and the qubit ground-state $|\text{III}\rangle = e_{1\downarrow}^\dagger e_{2\downarrow}^\dagger |0\rangle$.

The diagonal elements of the Hamiltonian for the first two states are

$$\begin{aligned} H_{\text{I,I}}^{(-3/2)} &= C_{\text{I}} + V_g - J_{13}, \\ H_{\text{II,II}}^{(-3/2)} &= C_{\text{II}} + 2V_g - J_{24}, \end{aligned} \quad (19)$$

where C_{I} is the sum of all single-particle energies and direct Coulomb interactions for state $|I\rangle$:

$$\begin{aligned} C_{\text{I}} &= E_1^e + E_2^e + E_3^e + E_3^h \\ &\quad + V_{1221}^{eeee} + V_{1331}^{eeee} + V_{2332}^{eeee} \\ &\quad - V_{1331}^{ehhe} - V_{2332}^{ehhe} - V_{3333}^{ehhe}, \end{aligned} \quad (20)$$

and similarly for C_{II} . The energies $J_{13} = V_{1313}^{eeee}$ and $J_{24} = V_{2424}^{eeee}$ are the intradot exchange interaction strengths, and all other exchange interactions are negligible.

In order that the excess electron can tunnel between the two configurations I and II, we set the voltage V_g across the device such that we align $H_{\text{I,I}}^{\downarrow\downarrow} = H_{\text{II,II}}^{\downarrow\downarrow} \equiv E^X$. This requires

$$\begin{aligned} V_g &= C_{\text{I}} - C_{\text{II}} - J_{13} + J_{24} \\ &= E_3^e - E_4^e + V_{1331}^{eeee} - V_{2442}^{eeee} + V_{2332}^{eeee} - V_{1441}^{eeee} \\ &\quad + V_{4334}^{ehhe} - V_{3333}^{ehhe} + J_{24} - J_{13}, \end{aligned} \quad (21)$$

which yields $V_g \approx 5$ meV for our parameters.

With this condition, the Hamiltonian for this sector reads

$$H^{(-3/2)} = \begin{pmatrix} E^X & -\tau_{34} & \Omega e^{-i\omega t} \\ -\tau_{34} & E^X & 0 \\ \Omega e^{i\omega t} & 0 & E^G \end{pmatrix}. \quad (22)$$

Moving to a basis of tunneling eigenstates for the exciton levels, $2^{-1/2}(|\text{I}\rangle \pm |\text{II}\rangle)$, we have

$$H^{(-3/2)} = \begin{pmatrix} E^X - \tau_{34} & 0 & \Omega e^{-i\omega t}/\sqrt{2} \\ 0 & E^X + \tau_{34} & \Omega e^{-i\omega t}/\sqrt{2} \\ \Omega e^{i\omega t}/\sqrt{2} & \Omega e^{i\omega t}/\sqrt{2} & E^G \end{pmatrix}. \quad (23)$$

We tune the laser frequency such that, apart from a small detuning δ , it is on resonance with the transition from the ground state and the lowest tunnel coupled exciton state with energy $E_X - \tau_{34}$:

$$\omega + \delta = E^X - \tau_{34} - E^G. \quad (24)$$

Finally, we move to a rotating frame

$$H^{(m)} \rightarrow H_R^{(m)} = R H^{(m)} R^\dagger + i\dot{R} R^\dagger, \quad (25)$$

with, in this case, $R = \text{Diag} \{ e^{i(\omega+E_G)t}, e^{i(\omega+E_G)t}, e^{iE_G t} \}$ to obtain

$$H_R^{(-3/2)} = \begin{pmatrix} \delta & 0 & \Omega/\sqrt{2} \\ 0 & \delta + 2\tau_{34} & \Omega/\sqrt{2} \\ \Omega^*/\sqrt{2} & \Omega^*/\sqrt{2} & 0 \end{pmatrix}. \quad (26)$$

We now consider the Hamiltonian, $H^{(-1/2)}$, for the sector in which the qubit spins have opposite directions. This is the important sector as it is here that the exchange between exciton and qubit electrons is manifest. Taking into account both electron tunneling and electron exchange, there are six exciton states in this sector. With intra-dot exchanges J_{13} and J_{24} diagonal, these are

$$\begin{aligned} |\text{I}\rangle &= e_{1\downarrow}^\dagger e_{2\uparrow}^\dagger e_{3\downarrow}^\dagger h_{3\uparrow}^\dagger |0\rangle, \\ |\text{II}\rangle &= 2^{-1/2} \left(e_{1\uparrow}^\dagger e_{2\downarrow}^\dagger e_{3\downarrow}^\dagger + e_{1\downarrow}^\dagger e_{2\downarrow}^\dagger e_{3\uparrow}^\dagger \right) h_{3\uparrow}^\dagger |0\rangle, \\ |\text{III}\rangle &= e_{1\uparrow}^\dagger e_{2\downarrow}^\dagger e_{4\downarrow}^\dagger h_{3\uparrow}^\dagger |0\rangle, \\ |\text{IV}\rangle &= 2^{-1/2} \left(e_{1\downarrow}^\dagger e_{2\uparrow}^\dagger e_{4\downarrow}^\dagger + e_{1\downarrow}^\dagger e_{2\downarrow}^\dagger e_{4\uparrow}^\dagger \right) h_{3\uparrow}^\dagger |0\rangle, \\ |\text{V}\rangle &= 2^{-1/2} \left(e_{1\uparrow}^\dagger e_{2\downarrow}^\dagger e_{3\downarrow}^\dagger - e_{1\downarrow}^\dagger e_{2\downarrow}^\dagger e_{3\uparrow}^\dagger \right) h_{3\uparrow}^\dagger |0\rangle, \\ |\text{VI}\rangle &= 2^{-1/2} \left(e_{1\downarrow}^\dagger e_{2\uparrow}^\dagger e_{4\downarrow}^\dagger - e_{1\downarrow}^\dagger e_{2\downarrow}^\dagger e_{4\uparrow}^\dagger \right) h_{3\uparrow}^\dagger |0\rangle. \end{aligned} \quad (27)$$

The first four states are degenerate under the intradot exchanges, and states 5 and 6 are split from the rest by an energy of $2J_{13} \approx 2J_{24} \approx 6.5$ meV. This means that they are effectively decoupled and can be neglected henceforth.

We can then proceed to the basis of tunneling eigenbasis defined by

$$\begin{aligned} |\text{I}'\rangle &= 1/\sqrt{6}|\text{I}\rangle + 1/\sqrt{3}|\text{II}\rangle + 1/\sqrt{6}|\text{III}\rangle + 1/\sqrt{3}|\text{IV}\rangle, \\ |\text{II}'\rangle &= 1/\sqrt{3}|\text{I}\rangle - 1/\sqrt{6}|\text{II}\rangle - 1/\sqrt{3}|\text{III}\rangle + 1/\sqrt{6}|\text{IV}\rangle, \\ |\text{III}'\rangle &= -1/\sqrt{3}|\text{I}\rangle + 1/\sqrt{6}|\text{II}\rangle - 1/\sqrt{3}|\text{III}\rangle + 1/\sqrt{6}|\text{IV}\rangle, \\ |\text{IV}'\rangle &= -1/\sqrt{6}|\text{I}\rangle - 1/\sqrt{3}|\text{II}\rangle + 1/\sqrt{6}|\text{III}\rangle + 1/\sqrt{3}|\text{IV}\rangle. \end{aligned} \quad (28)$$

In the basis of these four states plus the two ground states $e_{1\downarrow}^\dagger e_{2\uparrow}^\dagger$ and $e_{1\uparrow}^\dagger e_{2\downarrow}^\dagger$ the Hamiltonian in the rotating frame reads

$$H_R^{(-1/2)} = \begin{pmatrix} \delta & 0 & 0 & 0 & \Omega(t)/\sqrt{6} & \Omega(t)/\sqrt{6} \\ 0 & \delta + \tau_{34}^e/2 & 0 & 0 & \Omega(t)/\sqrt{3} & -\Omega(t)/\sqrt{12} \\ 0 & 0 & \delta + 3\tau_{34}^e/2 & 0 & -\Omega(t)/\sqrt{3} & \Omega(t)/\sqrt{12} \\ 0 & 0 & 0 & \delta + 2\tau_{34}^e & -\Omega(t)/\sqrt{6} & -\Omega(t)/\sqrt{6} \\ \Omega^*(t)/\sqrt{6} & \Omega^*(t)/\sqrt{3} & -\Omega^*(t)/\sqrt{3} & -\Omega^*(t)/\sqrt{6} & 0 & 0 \\ \Omega^*(t)/\sqrt{6} & -\Omega^*(t)/\sqrt{12} & \Omega^*(t)/\sqrt{12} & -\Omega^*(t)/\sqrt{6} & 0 & 0 \end{pmatrix}, \quad (29)$$

where the rotating frame is defined with frequency $\omega + E_G$ for all excited states and E_G for the two ground states.

Analysis of the final sector, in which both qubit spins point up, proceeds exactly as for $H^{(-1/2)}$ above, except with all electron spins flipped and only a single ground state $e_{1\uparrow}^\dagger e_{2\uparrow}^\dagger |0\rangle$. The resulting Hamiltonian, $H^{(1/2)}$, is the same as that of Eq. (29) but with the fifth state omitted.

Taking these results together, and ignoring for the moment the light-matter coupling, we see that the excitonic sector consists of four energy levels, of which the inside and outside pairs are doubly and triply degenerate, respectively. In each of these states the excitonic electron is delocalized over the entire structure, and is thus capable of mediating an exchange interaction between the qubits. Note that the optical coupling between these states and the qubit ground states shows a variety of different coupling strengths, as determined by the forefactors of Ω in the preceding Hamiltonians.

V. QUANTUM GATES

Having derived these Hamiltonians, we now show how the interactions they entail may be used to perform two-qubit operations. We begin by considering the system in the adiabatic limit in which the exciton levels are but virtually populated. This approach yields an effective gate operator U_{eff} acting only on the qubit space. Due to the complexity of the exciton structure, U_{eff} does not have the form of one of the standard QC gates. However, we give the relationship between U_{eff} and the controlled-phase (CPHASE) gate, which makes clear the QC capacity of U_{eff} . We then consider non-adiabatic operation of the system and show how this can improve operation times.

Second-order Rayleigh-Schrödinger perturbation theory of Raman processes can be used to derive an effective Hamiltonian for the qubit sector through the elimination

of the exciton levels. In the basis $\{|\downarrow\downarrow\rangle, |\downarrow\uparrow\rangle, |\uparrow\downarrow\rangle, |\uparrow\uparrow\rangle\}$ we obtain the effective Hamiltonian

$$\mathcal{H}_{\text{eff}} = -\frac{|\Omega(t)|^2}{\delta} \begin{pmatrix} x_1 & 0 & 0 & 0 \\ 0 & x_2 & y & 0 \\ 0 & y & x_3 & 0 \\ 0 & 0 & 0 & x_3 \end{pmatrix} = -\frac{|\Omega(t)|^2}{\delta} \hat{M} \quad (30)$$

with elements

$$\begin{aligned} x_1 &= \frac{\delta}{2} \left\{ \frac{1}{\delta} + \frac{1}{\delta + 2\tau_{34}^e} \right\}, \\ x_2 &= \frac{\delta}{6} \left\{ \frac{1}{\delta} + \frac{2}{\delta + \tau_{34}^e/2} \right. \\ &\quad \left. + \frac{2}{\delta + 3\tau_{34}^e/2} + \frac{1}{\delta + 2\tau_{34}^e} \right\}, \\ x_3 &= \frac{\delta}{12} \left\{ \frac{2}{\delta} + \frac{1}{\delta + \tau_{34}^e/2} \right. \\ &\quad \left. + \frac{1}{\delta + 3\tau_{34}^e/2} + \frac{2}{\delta + 2\tau_{34}^e} \right\}, \\ y &= \frac{\delta}{6} \left\{ \frac{1}{\delta} - \frac{1}{\delta + \tau_{34}^e/2} \right. \\ &\quad \left. - \frac{1}{\delta + 3\tau_{34}^e/2} + \frac{1}{\delta + 2\tau_{34}^e} \right\}. \quad (31) \end{aligned}$$

The validity of this Hamiltonian is conditioned on the standard adiabatic conditions of $T\delta/\hbar \gg 1$, with T the operation duration, to avoid populating the trion levels, and $|\Omega(t)|/\delta \ll 1$ such that perturbation theory is valid. Under these conditions, the time-evolution operator of the qubit sector may be approximated as $U_{\text{eff}}(t) \approx e^{-i\Lambda\hat{M}}$ with $\Lambda = -\int dt |\Omega(t)|^2/\hbar\delta$. We will use a Gaussian pulse shape, $\Omega(t) = A \exp(-t^2/2T^2)$, such that $\Lambda = -A^2\sqrt{\pi}T/\hbar\delta$. Evaluating the matrix exponential we find that U_{eff} can be written as

$$U_{\text{eff}} = \begin{pmatrix} e^{i\kappa_1} & 0 & 0 & 0 \\ 0 & e^{iq_-} \cos \Theta & -ie^{i(q_- + q_+)/2} \sin \Theta & 0 \\ 0 & -ie^{i(q_- + q_+)/2} \sin \Theta & e^{iq_+} \cos \Theta & 0 \\ 0 & 0 & 0 & e^{i\kappa_3} \end{pmatrix}. \quad (32)$$

where $\kappa_1 = -\Lambda x_1$, $\kappa_3 = -\Lambda x_3$, $\sin \Theta = \sin \phi \cos \theta$ with $\phi = \Lambda/2\sqrt{(x_2 - x_3)^2 + 4y^2}$ and $\tan \theta = (x_2 - x_3)/2y$, and where $q_{\pm} = \pm\chi - \Lambda(x_2 + x_3)/2$ with $\tan \chi = \sin \theta \tan \phi$.

As is evident, U_{eff} is not a standard QC gate. However, we now make the connection between U_{eff} and the familiar CPHASE gate

$$C(\Phi) = \text{Diag}(e^{i\Phi}, 1, 1, 1), \quad (33)$$

where Φ is the controlled phase. Let us define the single-qubit operation $S_i(\alpha) = \text{Diag}(e^{i\alpha}, 1)$ acting on qubit i , and the generalized SWAP gate

$$W(\Theta) = \begin{pmatrix} 1 & 0 & 0 & 0 \\ 0 & \cos \Theta & -i \sin \Theta & 0 \\ 0 & -i \sin \Theta & \cos \Theta & 0 \\ 0 & 0 & 0 & 1 \end{pmatrix}. \quad (34)$$

Setting $\Theta = \pi/2$ in $W(\Theta)$ yields a SWAP gate, and setting $\Theta = \pi/4$ gives a $\sqrt{\text{SWAP}}$ entangling gate. In terms of these operators the physical gate U_{eff} can be written as

$$U_{\text{eff}} = e^{i\kappa_3} S_1\left(\frac{q_- - \kappa_3}{2}\right) S_2\left(\frac{q_+ - \kappa_3}{2}\right) \times C(\Phi/2) W(\Theta) \times S_1\left(\frac{q_- - \kappa_3}{2}\right) S_2\left(\frac{q_+ - \kappa_3}{2}\right). \quad (35)$$

where

$$\begin{aligned} \Phi &= 2(\kappa_1 + \kappa_3 - q_- - q_+) \\ &= -4\Lambda y \\ &= \frac{2A^2\sqrt{\pi}T}{3\hbar} \left\{ \frac{1}{\delta} - \frac{1}{\delta + \tau_{34}^e/2} \right. \\ &\quad \left. - \frac{1}{\delta + 3\tau_{34}^e/2} + \frac{1}{\delta + 2\tau_{34}^e} \right\}. \quad (36) \end{aligned}$$

The gate U_{eff} therefore contains a product of two entangling operations, $C(\Phi/2)$ and $W(\Theta)$.

We can isolate the CPHASE gate from the product CW by observing that the key unitary transformation of W by the single-qubit operation $S'_2(\pi) = \text{Diag}(1, e^{-i\pi})$ gives $S'_2(\pi)W S'_2(\pi) = W^\dagger$. Since S'_2 commutes with C , the concatenation of CW and its transform yields,

$$C(\Phi/2)W(\Theta)S'_2(\pi)C(\Phi/2)W(\Theta)S'_2(\pi) = C(\Phi). \quad (37)$$

Note that the transformation is independent of Θ and can be carried out without the knowledge of its value. From this it follows that the composite operation of two applications of U_{eff} interspersed with appropriate single-qubit operations is equal to a CPHASE gate with the controlled phase Φ as defined in Eq. (36).

The entangling capability of U_{eff} can be assessed by calculating the concurrence \mathcal{C} of the states formed by acting with U_{eff} on a separable state of qubits 1 and 2, and averaging over all such inputs. This we find to be

$\overline{\mathcal{C}} = 1/8 |15 - 8 \cos(\Phi/2) \cos(2\Theta) - 7 \cos(4\Theta)|^{1/2}$, which depends only on the angles Φ and Θ . The average concurrence is thus bounded by $\frac{1}{2} |\sin(\Phi/4)| \leq \overline{\mathcal{C}} \leq \sqrt{11/32} \approx 0.586$, where the lower bound comes from the $\Theta = 0$ case. In the example that we consider later (operation 1 of Table I.), the off-diagonal angle is $\Theta = 0.42$ and the average concurrence is $\overline{\mathcal{C}} = 0.50$.

We will quantify the usefulness of gate U_{eff} for QC purposes solely through the CPHASE angle Φ , even though the gate U really requires two angles Φ and Θ to specify its entangling action completely. This one-parameter characterisation is appropriate because, from the foregoing, we know that knowledge of Φ sets a lower bound on the average entanglement generated by the gate. Furthermore, via the construction of Eq. (37), we know explicitly how to form a full CPHASE gate independent of the value of Θ , and indeed independent of the knowledge of its value. Clearly for U_{eff} to be an efficient gate we require Φ to be significant. A value of $\Phi = \pi$ gives the composite operation as a controlled- Z operation, and in which case the constituent U_{eff} operator may be said to be 'as efficient' as a $\sqrt{\text{SWAP}}$ gate, since two applications of $\sqrt{\text{SWAP}}$ are also required to form the controlled- Z operation [1]. Experimental demonstration of U_{eff} with $\Phi = \pi$ would, in this sense, be equivalent to the demonstration of a $\sqrt{\text{SWAP}}$ gate.

The question then becomes whether we can obtain a gate U_{eff} with a value of $\Phi = \pi$ within the time constraints set by T_Q and T_{Rel} . The answer is that if we insist that the evolution of the system be strictly adiabatic, then for a typical tunneling of $\tau_{34} = 0.05$ meV, such a gate takes several hundred picoseconds. At this coupling, we have $T_Q = 1.3$ ns, and so the adiabatic pulse time T is a significant fraction of T_Q , which is undesirable. However, if we allow a degree of non-adiabaticity in the time evolution, we can significantly reduce this operation time, as we now discuss.

If we populate the exciton levels then we require that the population is returned to the qubit sector at the end of the operation. We quantify the degree to which this happens with the average norm on the qubit space. Let us write as U_{total} the time-evolution operator of the total system. The corresponding operator for the qubit space is $U = P U_{\text{total}} P$, where P is the projector onto the 4x4 space. We can then define the average norm on the qubit space as $N_0 = \frac{1}{4} \sum_{i,j=1}^4 |U_{ij}|^2$. A perfect return has $N_0 = 1$ and in this case U necessarily has the same form as Eq. (32), given the Hamiltonian of Eq. (18).

We then numerically search the space of operations possible within the system for valid gate operations. For a given tunneling strength τ_{34} , pulse duration T , amplitude A , and detuning δ , we numerically integrate the time-dependent Schrödinger equation for the Hamiltonian of Eq. (18) to obtain the systems evolution from the four initial qubit states $\downarrow\downarrow, \downarrow\uparrow, \uparrow\downarrow$ and $\uparrow\uparrow$. From these results we can construct U , the evolution operator on the qubit space. We consider that the time-evolution can be construed as a valid gate if $N_0 \geq 0.99$.

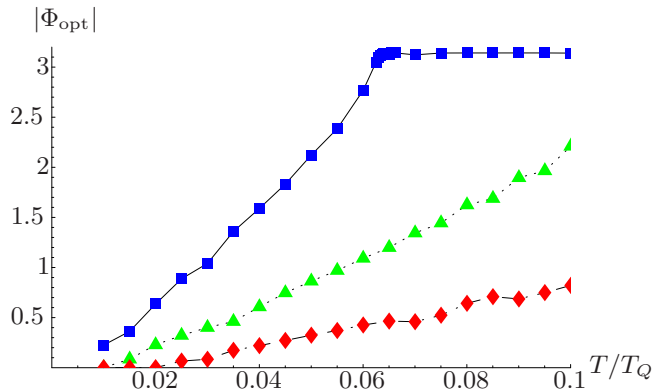


FIG. 3: (colour online) The absolute value of the optimal CPHASE angle Φ_{opt} as a function of T/T_Q , the pulse duration scaled by the qubit isolation time. Results are shown for three different tunnel strengths $\tau_{34} = 0.05$ meV (blue squares), $\tau_{34} = 0.1$ meV (green triangles), and $\tau_{34} = 0.2$ meV (red diamonds). As is evident, a phase of $\Phi = \pi$ can be obtained at $\tau_{34} = 0.05$ meV with $T/T_Q \gtrsim 0.064$. In real time units this equates to $T \approx 84$ ps. This value of Φ can also be achieved with higher tunneling amplitudes, but this requires longer pulses.

For a fixed pulse duration T , we obtain a range of valid gate operations with various different values of A and δ . From this set, we are interested in the gate with the most significant gating action which, in terms of the CPHASE angle described above, is the gate for which $|\Phi|$ is closest to π . We denote the CPHASE angle of the gate which fulfills the criteria at a given T as Φ_{opt} .

In Fig. 3 we plot the optimal angle Φ_{opt} as a function of pulse duration T for several different tunnel amplitudes τ_{34} . Let us consider the $\tau_{34} = 0.05$ meV case. The angle Φ_{opt} reaches a value of π at a value of $T/T_Q = 0.064$ and then saturates. At this coupling, $T_Q = 1.3$ ns and so the pulse duration is $T = 84$ ps, which is short compared with both T_Q and T_{rel} . For the higher couplings shown in Fig. 3, we obtain $\Phi_{\text{opt}} = \pi$ only for ratios $T/T_Q > 0.1$.

In Table I, we give parameters and results for two example $\tau_{34} = 0.05$ meV operations: the first corresponds to the minimum pulse time T required to obtain $\Phi = \pi$, and the second is a longer duration pulse with higher norm N_0 . In the course of the evolution with the first set of parameters, the exciton states are occupied with a peak population of the order of 40%. For initial conditions of three of the four basis states virtually no population is left in the trion levels at the conclusion of this operation. However, evolution from $\downarrow\uparrow$ does leave a small remnant and this reduces the qubit norm to its value of $N_0 = 0.991$. For longer pulse durations, as in the second operation of Tab. I, this remnant can be eliminated.

Permitting the system to evolve non-adiabatically then improves the performance of the gate by reducing the time required to perform a useful rotation.

	τ_{34}	T	T/T_Q	δ	A	Φ	N_0	\mathcal{F}_{Rel}
1	0.05	84	0.064	0.0729	0.10983	3.1415	0.991	0.970
2	0.05	125	0.095	0.084	0.078025	3.1415	0.99993	0.984

TABLE I: Parameters and results for two example operations. τ_{34} is the tunneling amplitude between dots, and A , T , and δ are the amplitude, duration and detuning of the laser pulse. The units of τ_{34} , δ and A are meV, and T is measured in ps. For both operations $\Phi \approx \pi$, as require. Without spontaneous emission the fidelity is equal to the norm on the qubit space $\mathcal{F} = N_0$ and this can be made very close to unity, as in the second operation. In the presence of spontaneous emission, the fidelity \mathcal{F}_{rel} is slightly reduced.

VI. HOLE-MIXING AND SPONTANEOUS EMISSION

Other than the direct and kinetic exchanges between the qubits discussed above, there are two further deleterious processes that we now discuss: hole-mixing and spontaneous emission. As we know from the Luttinger-Kohn model of semiconductor bands [12, 13], hole-mixing means that, rather than the ‘bare’ heavy-hole states $|\frac{3}{2}, \pm \frac{3}{2}\rangle$, the actual hole states are better approximated by

$$|H^\pm\rangle = \cos\theta|\frac{3}{2}, \pm \frac{3}{2}\rangle - \sin\theta e^{\mp i\phi}|\frac{3}{2}, \mp \frac{1}{2}\rangle, \quad (38)$$

where $|\frac{3}{2}, \mp \frac{1}{2}\rangle$ are light-hole states, and θ_m , ϕ_m are mixing angles. With this mixing, the light-matter interaction Hamiltonian becomes

$$H_{\text{int}} = \Omega(t)e^{-i\omega t} \left\{ \cos\theta_m e_{3\downarrow}^\dagger h_{3H^+}^\dagger - \sqrt{1/3}e^{i\phi_m} \sin\theta_m e_{3\uparrow}^\dagger h_{3H^-}^\dagger \right\} + \text{H.c.}, \quad (39)$$

where the factor of $\sqrt{1/3}$ in the second term comes from the different weights of in-plane components of the valence-band wave functions [13, 14].

This interaction requires that we consider an extra excited-state sector with $|H^- \rangle$ instead of $|H^+ \rangle$. Taking both sectors into account, we can readily derive an effective Hamiltonian in the presence of hole mixing. We find

$$\mathcal{H}_{\text{mix}} = \cos^2\theta_m \mathcal{H}_{\text{eff}} + \frac{1}{3} \sin^2\theta_m \mathcal{H}_-, \quad (40)$$

where \mathcal{H}_{eff} is as in Eq. (30) and

$$\mathcal{H}_- = -\frac{\Omega^2}{\delta} \begin{pmatrix} x_3 & 0 & 0 & 0 \\ 0 & x_3 & y & 0 \\ 0 & y & x_2 & 0 \\ 0 & 0 & 0 & x_1 \end{pmatrix}, \quad (41)$$

with terms as in Eq. (31). Note that the hole-mixing does not introduce any new matrix elements interactions between qubit states that were not already present in the

non-hole-mixing Hamiltonian. From this and the symmetry of \mathcal{H}_{mix} it immediately follows that the CPHASE angle is $\Phi_{\text{mix}} = \{\cos^2 \theta_m + \frac{1}{3} \sin^2 \theta_m\} \Phi$, where Φ is the original angle of Eq. (36). Thus, the effect of hole-mixing is to slightly decrease the CPHASE angle Φ , and this can simply be compensated for by a proportionate increase in Rabi frequency Ω .

We now consider spontaneous emission. Given our laser excitation and the magnitudes of the indirect oscillator strengths, the dominant spontaneous emission path is the direct recombination of exciton pair $e_{3\downarrow}^\dagger h_{3\uparrow}^\dagger$. As noted previously, the time-scale of this process is of the order of $T_{\text{rel}} = 1$ ns. We can assess the effects through the numerical integration of the master equation for the system in the Lindblad form.

We judge the quality of the operation in the presence of spontaneous emission through the fidelity [15, 16], defined as

$$\mathcal{F} = \overline{\langle \Psi_{\text{in}} | \tilde{U}^\dagger \rho_{\text{out}} \tilde{U} | \Psi_{\text{in}} \rangle}, \quad (42)$$

where the overline represents an average over all input states $|\Psi_{\text{in}}\rangle$, ρ_{out} is the output density matrix given $|\Psi_{\text{in}}\rangle$, and \tilde{U} is the ideal gate operation. We define \tilde{U} by taking the gate operator without spontaneous emission and renormalising it such that $N_0 = 1$. Correspondingly, the fidelity of the operation U without spontaneous emission is simply given by $\mathcal{F} = N_0$.

The results of these calculations can be appreciated by again studying the two operations listed in Table I. In this table we give the fidelities in the presence of spontaneous emission. For the first, shorter pulse, spontaneous emission reduces the fidelity from 0.99 to 0.97. For the longer pulse, fidelity is reduced from very close to unity to 0.984. This final value is typical for operations with spontaneous emission, with the final fidelity lying in the 98–99% range.

This reduction in fidelity arises largely from population being left in the trion levels, as attested by the fact that the norm on the qubit space is affected to a similar extent. This residual population occurs because the spontaneous emission removes the direct exciton $e_3 h_3$ but leaves the indirect exciton $e_4 h_3$ untouched. Since, after the laser pulse has passed, this indirect state has no route back to the ground state, it is effectively trapped. This population eventually returns to the ground state, through either interdot tunneling plus direct spontaneous emission or, to a lesser extent, indirect emission, but this occurs on a time scale greater than that considered here. This trapping effect, although ever present, is small enough that operations of sufficient quality can still be obtained.

VII. SINGLE-QUBIT ROTATIONS

An important feature of the current set-up is that it is compatible with single-qubit operations on the electron spins. As described in Ref. [14] (see also Ref. [16]), single

qubit operations can be performed through the excitation of an exciton in the ground-state levels of a single dot (e.g. the levels 1 in dot A). The addressability of the individual dots is assured here by their different Darwin radii. To obtain arbitrary rotations, a static magnetic field is required in the x -direction (perpendicular to the growth direction), and it is important that the two-qubit operations function correctly in the presence of this field.

In InAs dots, both the electron and hole g -factors are finite [17, 18], and this leads to a splitting of the single-dot trion levels and the linear polarization of the optical transitions [14, 17]. Assuming that both g -factors have the same sign, we can perform our two-qubit operations with a \mathbf{H} -polarized laser (as defined in Refs. [14, 17]) rather than a σ_+ -circularly polarized one. We then derive an effective Hamiltonian for this situation and find

$$\mathcal{H}_B = \frac{1}{2} \{ \mathcal{H}_{\text{eff}} + \mathcal{H}_- (\delta + \Sigma_B) \}. \quad (43)$$

where the second term is the same as Eq. (41) but with the detuning δ replaced by $\delta + \Sigma_B$ throughout. Here $\Sigma_B = (g_x^e + g_x^h) \mu_B B_x$, with g_x^e and g_x^h the electron and hole in-plane g -factors, B_x the in-plane field, and μ_B the Bohr magneton. As with the hole-mixing, we see that the magnetic field does not add any new matrix elements between qubit states, and thus the operation has the same character as before. Now, however, the CPHASE angle is given by $\Phi_B = 1/2 \{ \Phi + \Phi(\delta + \Sigma_B) \}$, where the second term is the same as Eq. (36) but with $\delta + \Sigma_B$ replacing δ throughout. The contribution of this term is expected to be small since, with g -factors $|g_x^e| = 0.46$ and $|g_x^h| = 0.29$ [17, 18], at $B = 8$ T, we have $|\Sigma_B| \approx 0.4$ meV which is larger than typical values of δ . In any case, these changes to Φ can easily be compensated for by a trivial change in amplitude of the laser.

VIII. CONCLUSIONS

We have described a mechanism for obtaining optical-controlled quantum gates in quantum dots. This may be thought of as a confined ORKKY interaction in which the exchange between the two qubit spins is mediated by a set of exciton states delocalized over the double dot structure.

For this gating to function it is imperative that the two dots be spaced an appropriate distance apart such that the tunnel coupling between them is small enough that the kinetic exchange can be neglected over the course of a gate operation, but large enough that laser pulses short enough compared with exciton relaxation time can be used. Our calculations show that a distance of $d \approx 8$ nm would be ideal. In this case, significant gates (equivalent to $\sqrt{\text{SWAP}}$) can be obtained at high fidelities with pulse durations of the order of 100ps.

The speed of this operation is essentially limited by the occurrence of the kinetic exchange. Without this effect, the dots could be closer together, the tunneling matrix

elements larger, and hence the strength of the gating interaction much stronger. However, this exchange is unavoidable in vertically-stacked QDs, since such dots only grow in a stack when the separation between the two dots is small [19]. This problem, therefore, is not unique to our gating mechanism, but rather a feature of coupled QDs, and any proposal seeking to show controlled quantum operations in such a structure must take it into account.

In this respect, horizontally-coupled quantum dots have an advantage since, as such dots are coupled in the xy plane, the overlap of the excited states is a factor of $\sqrt{2}$ greater than that of the ground states. This means that the strength of the kinetic exchange interaction is reduced by a factor of one-half relative to exciton-tunneling. This in turn means that pulse-durations half that described here can be used to obtain the same results.

We have also demonstrated that our two-qubit operations function equally as well with an in-plane magnetic field. This is important because it shows that our set-up is compatible the single-qubit rotations of Ref. [14]. In combination, this means that we have demonstrated that the laser excitation of excitonic states provides a realistic, experimentally-accessible protocol for the fast performance of a universal set of quantum operations on two electron-spin-qubits in a coupled double quantum dot.

This work was supported by ARO/NSA-LPS.

APPENDIX A: SINGLE PARTICLE WAVE FUNCTIONS

Our single-particle variational wave functions are separable into z and xy components. In the z direction, the wave functions are those of ground state of a square well of depth V_0 and width $2a$:

$$\chi(z) = \begin{cases} C \exp(\beta z) & z < -a, \\ B \cos(\alpha z) & |z| \leq a, \\ C \exp(-\beta z) & z > a. \end{cases} \quad (\text{A1})$$

where

$$\alpha = \sqrt{\frac{2m_e E_z}{\hbar^2}}, \quad (\text{A2})$$

$$\beta = \sqrt{\frac{2m_e(V_0 - E_z)}{\hbar^2}}. \quad (\text{A3})$$

The ground-state energy E_z may be found through solution of the equation

$$\alpha \tan(\alpha a) = \beta. \quad (\text{A4})$$

In the xy plane we have the ground-state and first excited-state Fock-Darwin orbitals

$$\eta_s(\omega; \rho, \theta) = \sqrt{\frac{\omega}{\pi}} e^{-\frac{1}{2}\omega\rho^2}, \quad (\text{A5})$$

$$\eta_{p\pm}(\omega; \rho, \theta) = \frac{\omega}{\sqrt{\pi}} \rho e^{-\frac{1}{2}\omega\rho^2} e^{\mp i\theta}, \quad (\text{A6})$$

with $\lambda = m\omega/\hbar$. Since the two p -orbitals are degenerate, and angular momentum is conserved, we only need consider a single orbital and choose $\eta_p = \eta_{p+}$ for concreteness.

The four complete wave functions $\phi_i(\mathbf{r})$ are given in Eq. (4), but these are nonorthogonal. As our variational basis we therefore use

$$\begin{aligned} \psi_1(\mathbf{r}) &= \gamma_1^{-1} \{ \phi_1(\mathbf{r}) - g_1 \phi_2(\mathbf{r}) \}, \\ \psi_2(\mathbf{r}) &= \gamma_1^{-1} \{ \phi_2(\mathbf{r}) - g_1 \phi_1(\mathbf{r}) \}, \\ \psi_3(\mathbf{r}) &= \gamma_3^{-1} \{ \phi_3(\mathbf{r}) - g_3 \phi_4(\mathbf{r}) \}, \\ \psi_4(\mathbf{r}) &= \gamma_3^{-1} \{ \phi_4(\mathbf{r}) - g_3 \phi_3(\mathbf{r}) \}, \end{aligned} \quad (\text{A7})$$

which are all orthogonal. Here, the overlaps S_{ij} are defined $S_{ij} = \int d^3\mathbf{r} \phi_i(\mathbf{r})\phi_j(\mathbf{r})$, and the normalization coefficients are given by

$$\begin{aligned} g_1 &= \left(1 - \sqrt{1 - S_{12}^2} \right) / S_{12}, \\ g_3 &= \left(1 - \sqrt{1 - S_{34}^2} \right) / S_{34}, \\ \gamma_1 &= \sqrt{1 - 2g_1 S_{12} + g_1^2}, \\ \gamma_3 &= \sqrt{1 - 2g_3 S_{34} + g_3^2}. \end{aligned} \quad (\text{A8})$$

-
- [1] D. Loss and D. P. DiVincenzo, Phys. Rev. A **57**, 120 (1998).
[2] G. Burkard, G. Seelig, and D. Loss, Phys. Rev. B **62**, 2581 (2000).
[3] T. Calarco, A. Datta, P. Fedichev, E. Pazy, and P. Zoller, Phys. Rev. A **68**, 012310 (2003).
[4] M. Feng, I. D'Amico, P. Zanardi, and F. Rossi, Europhys.

- Lett., **66**, 14 (2004).
[5] B. W. Lovett, A. Nazir, E. Pazy, S. D. Barrett, T. P. Spiller, and G. A. D. Briggs, Phys. Rev. B **72**, 115324 (2005).
[6] G. Ortner, I. Yugova, G. Baldassarri Hger von Hgersthal, A. Larionov, H. Kurtze, D. R. Yakovlev, M. Bayer, S. Fafard, Z. Wasilewski, P. Hawrylak, Y. B. Lyanda-Geller,

- T. L. Reinecke, A. Babinski, M. Potemski, V. B. Timofeev, and A. Forchel, *Phys. Rev. B* **71**, 125335 (2005).
- [7] E. A. Stinaff, M. Scheibner, A. S. Bracker, I. V. Ponomarev, V. L. Korenev, M. E. Ware, M. F. Doty, T. L. Reinecke, and D. Gammon, *Science* **311**, 636 (2006).
- [8] C. Piermarocchi, P. Chen, and L. J. Sham, *Phys. Rev. Lett.* **89**, 167402 (2002); C. Piermarocchi and G. F. Quinteiro, *Phys. Rev. B* **70**, 235210 (2004).
- [9] G. Ramon, Y. Lyanda-Geller, T. L. Reinecke, and L. J. Sham, *Phys. Rev. B* **71**, 121305 (2005).
- [10] S. Cortez, O. Krebs, S. Laurent, M. Senes, X. Marie, P. Voisin, R. Ferreira, G. Bastard, J-M. Gerard, and T. Amand, *Phys. Rev. Lett.* **89**, 207401 (2002).
- [11] M. E. Ware, E. A. Stinaff, D. Gammon, M. F. Doty, A. S. Bracker, D. Gershoni, V. L. Korenev, S. C. Badescu, Y. Lyanda-Geller, and T. L. Reinecke, *Phys. Rev. Lett.* **95**, 177403 (2005).
- [12] J. M. Luttinger and W. Kohn, *Phys. Rev.* **97**, 869 (1955).
- [13] D. A. Broido and L. J. Sham, *Phys. Rev. A* **31**, 888 (1985).
- [14] C. Emary and L. J. Sham, *J. Phys.: Condens. Matter* **19**, 056203 (2007).
- [15] J. F. Poyatos, J. I. Cirac, and P. Zoller, *Phys. Rev. Lett.* **78**, 390 (1997).
- [16] Pochung Chen, C. Piermarocchi, L. J. Sham, D. Gammon, and D. G. Steel, *Phys. Rev. B* **69**, 075320 (2004).
- [17] C. Emary, Xiaodong Xu, D. G. Steel, S. Saikin, L. J. Sham, *Phys. Rev. Lett.* **98**, 047401 (2007).
- [18] Xiaodong Xu *et al.*, (unpublished).
- [19] Q. Xie, A. Madhukar, P. Chen, and N. P. Kobayashi, *Phys. Rev. Lett.* **75**, 2542 (1995).